Journal of the Korean Electrochemical Society
Vol. 10, No. 4, 2007, 252-256

Rate Capability of Electric Double-Layer Capacitor (EDLC) Electrodes According to Pore Length in Spherical Porous Carbons

Bok H. Ka, Songhun Yoon, and Seung M. Oh*

Department of Chemical and Biological Engineering, and Research Center for Energy Conversion & Storage, Seoul National University, Seoul 151-774, Korea

(Received September 27, 2007 : Accepted October 18, 2007)

Abstract : A series of spherical porous carbons were prepared *via* resorcinol-formaldehyde (*RF*) sol-gel polymerization in the presence of cationic surfactant (CTAB, cetyltrimethylammonium bromide), wherein the carbon sphere size was controlled by varying the CTAB introduction time after a pre-determined period of addition reaction (termed as "pre-curing"). The sphere size gradually decreases with an increase in the pre-curing time within the range of 30-150 nm. The carbons possess two types of pores; one inside carbon spheres (intra-particle pores) and the other at the interstitial sites made by carbon spheres (inter-particle pores). Of the two, the surface exposed on the former was dominant to determine the electric double-layer capacitor (EDLC) performance of porous carbons. As the intra-particle pores were generated inside RF gel spheres by gasification, the pore diameter was similar for all these carbons, thereby the pore length turned out to be a decisive factor controlling the EDLC performance. The charge-discharge voltage profiles and complex capacitance analysis consistently illustrate that the smaller-sized RF carbons deliver a better rate capability, which must be the direct result of facilitated ion penetration into shorter pores.

Keywords : Electric double-layer capacitors; Resorcinol-formaldehyde polymerization; Complex capacitance analysis; Porous carbons; Surfactants

1. Introduction

Electric double-layer capacitors (EDLC) are electric energy-storage devices that can store and deliver energy at high rates, also with longer cycle life, beyond those accessible by modern secondary batteries.[1,2] This feature largely comes from the fact that the charge storage in EDLC takes place at electrified electrode surface by simple electrostatic charge separation mechanism, which is contrasted by bulk chemical reactions (for instance, ion intercalation) involved in secondary batteries.[3-5]

At present, activated carbons are the favoured choice for EDLC electrode materials as they have high electric conductivity and large surface area, which allows high charge-storage ability (capacitance). The rate capability, which is reflected as *RC* time constants, is another important consideration in EDLC electrodes, where *R* and *C* denote the equivalent series resistance (ESR) and capacitance, respectively.[6,7] To have smaller *RC* time constants (that is, better rate capability), one should minimize either capacitance or ESR. Minimization of ESR is, however, the better choice because capacitance is an important consideration for EDLC electrodes. In general, ESR is the summation of electrode resistance, bulk electrolyte resistance and electrolyte resistance within pores. In common EDLC electrodes, the pore resistance is dominant in magnitude over the others unless the electrode materials and electrolytes are highly resistive, thereby the pore resistance should be minimized to achieve a high rate capability. Along this line, the pore structure (pore size, length, and connectivity) of EDLC electrode materials should be optimized: Too small pores in size are not desirable since ionic motions are sluggish in such small pores. On aspect of pore length, shorter pores are favoured because ion diffusion in and out of pores is more facilitated.

In this paper, we present the experimental data ascertaining that carbons carrying a shorter pore length deliver a high rate capability. This was possible since a series of spherical porous carbons prepared in this work differ in the sphere size but are similar in the pore diameter, leaving the pore length to be the decisive factor controlling the rate capability. The size control of spherical carbons was accomplished by changing the pre-curing time in the resorcinol-formaldehyde (RF) sol-gel polymerization step.[8-10] The rate capability of porous carbon electrodes was characterized by charge-discharge cycling and complex capacitance analysis.[7,11,12]

2. Experimental

2.1. Preparation and characterization

A mixture of resorcinol (*R*, Aldrich Chem. Co., 98%), formaldehyde (*F*, Aldrich Chem. Co, 37%), and Na_2CO_3 (as a catalyst) (50:100:1 in molar ratio) was reacted at 50°C with stirring. After a certain period of reaction (pre-curing), the surfactant solution (molar ratio of CTAB:H_2O = 1 : 350) was

*E-mail: seungoh@snu.ac.kr

added into the reactant mixture (molar ratio of *R*:CTAB = 7 : 1). The reaction mixture was then vigorously stirred for additional 2 h and aged for a week at 85°C. The resulting precipitate (RF/CTAB) was washed with de-ionized water to remove the residual Na_2CO_3, and dried in air at 85°C to obtain the RF gels. The porous carbons were obtained after carbonizing the gels at 700°C for 1 h under Ar atmosphere.

Morphology of the porous carbons was examined using a field-emission scanning electron microscopy (FE-SEM, JEOL JSM-6700F). Surface area and pore size distribution (PSD) were analyzed from the N_2 and Ar adsorption isotherms with a gas adsorption analyzer (Micromeritics, ASAP 2020).

2.2. Characterization of RF carbon electrodes

To prepare the EDLC electrodes, a mixture of porous carbon, polytetrafluroethylene (PTFE as a polymeric binder) and Ketjenblack ECP-600JD (as a carbon additive for conductivity enhancement) was dispersed in *iso*-propyl alcohol and coated on stainless steel Exmet that was used as the current collector. The electrode plate was dried at 120°C for 12 h and pressed to enhance the inter-particle contact and to ensure a better adhesion to the current collector. The electrochemical performance of RF carbon electrodes was analyzed with a three-electrode configuration in aqueous 2.0 *M* H_2SO_4 electrolyte. A Pt flag and saturated Ag/AgCl was used as the counter and reference electrode, respectively. Galvanostatic charge-discharge voltage profiles were obtained at a current density of 20 mA cm^{-2}. AC impedance measurement was made over the frequency range of 100 kHz –5 mHz (Zahner, im6e) with an ac amplitude of 5 mV. Experimental data were processed and analyzed with Zview 2 (Scribner Associates, Inc.) and Mathcad 2000 Professional (MathSoft, Inc.) software.

3. Results and discussion

3.1. Preparation and characterization of RF carbons

The RF sol-gel polymerization is composed of two consecutive reactions: (i) The formation of hydroxymethyl derivatives of resorcinol that are generated by formaldehyde addition to the hydrogen-abstracted resorcinol and (ii) condensation of the hydroxymethyl derivatives and cluster growth.[13-20] The former is base-catalyzed and the latter by acids. It is thus very likely that the solution pH is a critical factor controlling the reaction kinetics. The solution pH was monitored in the course of RF polymerization in this work (Fig. 1). In the normal RF polymerization without CTAB addition, the pH decreases slightly from 7.3 to 5.7 until the gel is precipitated. Interestingly, however, rapid pH drop is observed upon addition of CATB (the trace of RF00). It is also found that the solution pH drops to a lower value when a larger amount of CTAB is added. This pH drop can be accounted for by the electrostatic organic-organic interaction proposed by Nishiyama and his co-workers who conducted a similar RF polymerization in the presence of CTAB.[9] On the basis of x-ray diffraction analysis, they proposed that the cationic heads of CTAB combine with anionic functional group of RF clusters by a lipophilic interaction. Here, the anionic functional group is the oxygen anions generated from the phenolic or hydroxymethyl groups after releasing protons. Even if Nishiyama did not explicitly mention the proton release, the solution pH should be decreased if this lipophilic interaction is indeed occurring.

The observation that CTAB addition during the course of RF polymerization leads to a rapid pH drop allowed us to develop an idea to control the size of RF gel particles. The idea was to allow the base-catalyzed addition reaction for a pre-determined period of time in advance (pre-cured), and then enforce the acid-catalyzed condensation reaction by adding CTAB. A simple expectation was that a larger number of gel particles but of a smaller size can be obtained by extending the pre-curing time since the base-catalyzed addition reaction is extended at higher pH (>6.0) to generate a larger number of hydroxymethyl derivatives that will eventually be

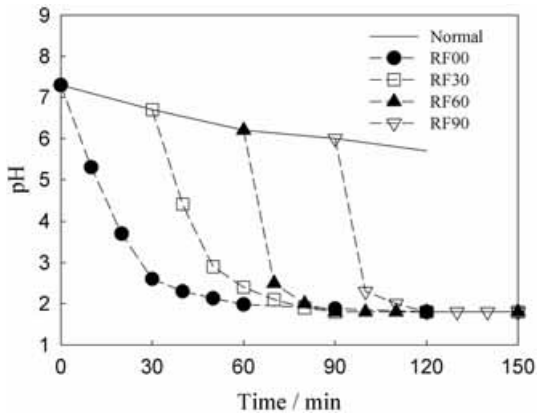

Fig. 1. Evolution of the solution pH in the course of normal RF polymerization and upon CTAB addition after a pre-determined period of pre-curing: RF00; without pre-curing, RF30; 30 min pre-curing, RF60; 60 min, and RF90; 90 min. Note a rapid pH drop upon CTAB addition.

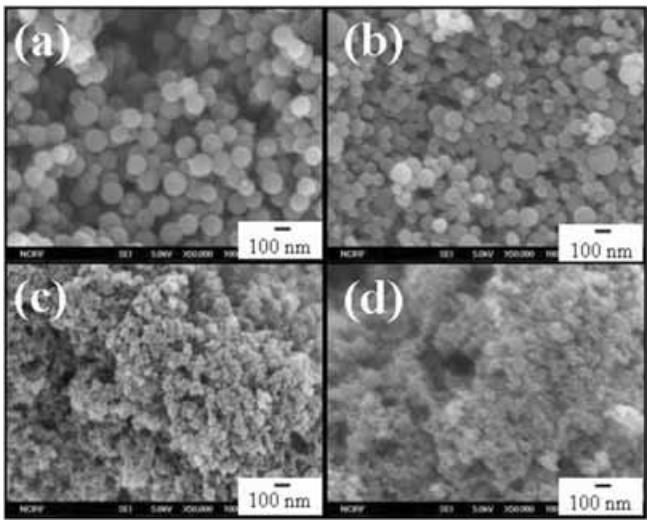

Fig. 2. FE-SEM images of RF carbons as a function of pre-during time: (a); RF00, (b); RF30, (c); RF60, and (d); RF90. Note that the RF carbons carry a sphere shape, whose diameter steadily decreases with an increase in the pre-curing time.

condensed by acids generated upon CTAB addition. In Fig. 1, the evolution of solution pH is displayed, where it is seen that the solution pH drops rapidly whenever CTAB is added. In the inset, the pre-curing time is indicated as the numbers.

Fig. 2 shows the field-emission scanning electron microscopy (FE-SEM) images of RF carbons that were prepared with a variation in the pre-curing time while the other variables being fixed. Note that the RF gel samples before carbonization show a similar morphology except for having a slightly larger sphere size, thus omitted. The most revealing feature in Fig. 2 is that the size of carbon particles successively decreases with an increase in the pre-curing time, which is what is expected. The particle diameter is around 150 nm for RF00 (without pre-curing), but decreases down to 30 nm for RF90 (pre-cured for 90 min). Additional feature found in Fig. 2 is that the individual carbon particle carries a spherical shape and they are agglomerated to generate pores at the interstitial sites (inter-particle pores). These carbons also carry the pores inside carbon spheres (intra-particle pores) as presented later.

By summarizing the experimental data presented above, the role of surfactant molecules in this synthesis is identified as follows[8-10] : First, the surfactant molecules act as a template for the RF polymerization. That is, the CTAB molecules form spherical micelles immediately after being added into the reaction mixture, into which the hydroxymethyl derivatives that are generated during the pre-curing and monomers move and then grow as sphere-shaped gel particles, which are further three-dimensionally connected via a cross-linking reaction. As a result, interstitial sites are generated that eventually become the inter-particle pores. Second, the surfactant molecules that are adsorbed on the inter-particle pore walls lower the surface tension at the pore water-gel interface so as to minimize the pore collapse during the drying step, giving rise to a stable inter-particle pore structure. Finally, some of CTAB molecules likely penetrate into the core region of CTAB micelles and lipophilically interact with the gel clusters to produce protons.

Fig. 3 shows the pore size distribution calculated by the BJH (Barrett-Joyner-Halenda) method from the adsorption branch of nitrogen isotherms. Upon considering that the pore size is in the range of a few tens to a few hundreds nanometers and the pores become narrower with an increase in the pre-curing time, we can reach a conclusion that these pores are developed at the interstitial sites made by the carbon spheres (inter-particle pores). In the inset, the pore size distribution calculated by the HK (Horvath-Kawazoe) method from the adsorption branch of argon isotherms is provided.[21,22] A very similar pore size distribution was observed in the range of 0.5-2.0 nm regardless of the carbon samples. The much smaller diameter (< 2 nm) for these pores than that for the inter-particle pores and absence of these pores in the gel samples illustrate that they are generated inside the RF gel spheres as a result of gasification in the carbonization process (intra-particle pores).

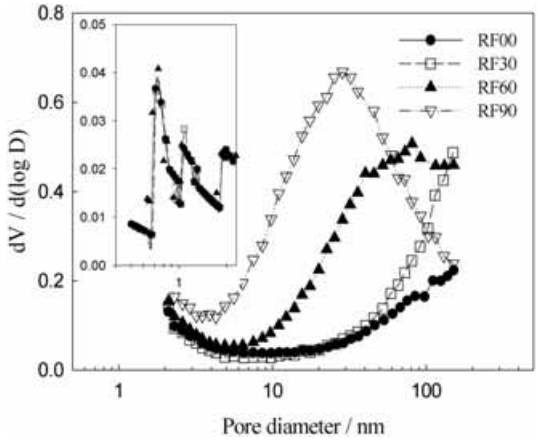

Fig. 3. Pore size distribution (PSD) that was calculated by the BJH method from the nitrogen adsorption isotherms. The PSD derived from the argon adsorption isotherms is provided in the inset. Note that the diameter of inter-particle pores decreases with an increase in the pre-curing time, whereas the diameter of intra-particle pores is largely the same for four RF carbons.

Table 1 lists the total surface area (S_{tot}) and total pore volume (V_{tot}) that were obtained by using the BET (Brunauer-Emmett-Teller) method. The volume (V_{mic}) and surface area (S_{mic}) relevant to micropores (< 2 nm) that were obtained from the *t*-plot method are also listed.[23-25] Note that the S_{ext} denotes the surface area exposed on the inter-particle pores (> 2.0 nm). The most informative feature here is that the contribution of S_{mic} is dominant for the total surface area (S_{tot}), ensuring that the EDLC performance of these carbons is determined by the intra-particle pores. In addition, the insignificant difference in the V_{mic} values between the samples supports that the micropores are developed inside carbon spheres. The larger difference in the values of total surface area (S_{tot}) and total pore volume (V_{tot}) between the samples can then be ascribed to a contribution from the inter-particle pores.

3.2. Rate capability of RF carbon EDLC electrodes

When account is taken of the similar pore diameter for intra-particle pores between the samples (the inset in Fig. 3), it is seemingly that ion penetration into the intra-particle

Table 1. Surface area and pore volume of RF carbons as a function of pre-curing time in the RF polymerization step

	S_{tot}[a]/$m^2\,g^{-1}$	V_{tot}[a]/$m^2\,g^{-1}$	S_{ext}[b]/$m^2\,g^{-1}$	S_{mic}[b]/cm^3g^{-1}	V_{mic}[b]/$cm^3\,g^{-1}$
RF00	472	0.40	90	382	0.18
RF30	515	0.47	103	412	0.19
RF60	592	0.65	185	407	0.19
RF90	657	0.92	231	426	0.20

[a] Obtained from BET method.
[b] Obtained from *t*-plot method.

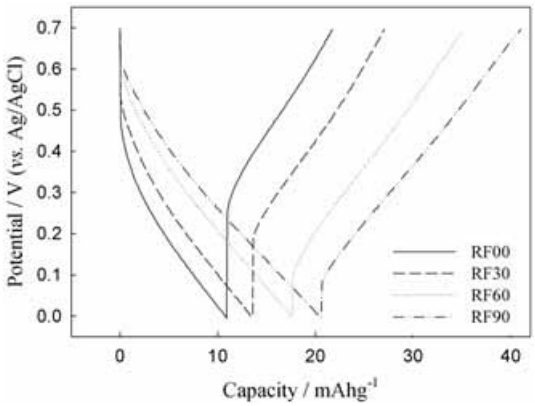

Fig. 4. Galvanostatic charge-discharge voltage profiles recorded with the RF carbon electrodes. Note the voltage drop at the very earlier period of charge-discharge switching, which reflects the magnitude of equivalent series resistance (ESR).

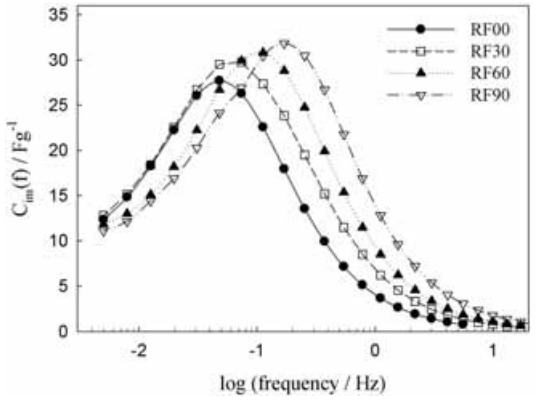

Fig. 5. Imaginary capacitance plots derived from the ac impedance data. Note the successive increase in the peak frequency with an increase in the pre-curing time in the RF polymerization step, which indicates a progressive decrease in the RC time contant and enhanced rate capability.

pores becomes more facilitated for the RF carbons pre-cured for longer period of time because the pore length is shorter with a decrease in carbon sphere size. With this in mind, the rate capability of EDLC electrodes fabricated with the RF carbons was studied. Fig. 4 provides the galvanostatic charge-discharge voltage profiles for four different RF carbon electrodes, where the downward profiles correspond to charging (charge storage) and the upward ones to discharging (charge removal from the electrodes). It is apparent in Fig. 4 that the voltage drop at the very earlier period of charge-discharge switching becomes smaller with an increase in the pre-curing time (i.e., with a decrease in the carbon sphere size). Table 2 lists the ohmic resistance values that were calculated from the voltage drops. This ohmic voltage drop certainly reflects the ESR in these cells, which is the summation of electrode resistance ($R_{electrode}$), bulk electrolyte resistance ($R_{electrolyte}$) and electrolyte resistance within pores (R_{pore}). Note that $R_{electrode}$ was very small and largely the same for the electrodes (ca. 7 $\times 10^{-3}$ Ωg) in this work and $R_{electrolyte}$ should be comparable to each other becasue the same cell configuration was used. It is thus very likely that R_{pore} is the dominant and meaningful variable to affect the magnitude of overall ESR. Note that several previous reports have already demonstrated that the resistance relevant to ion penetration into intra-particle pores is the dominant factor determining the overall ohmic resistance.[5-7,26-28] Given that the surface area exposed on the intra-particle pores is dominant (Table 1), such that the EDLC performance is predominantly determined by the pore structure of intra-particle pores, the smaller ohmic resistance observed with the carbons pre-cured for longer period of time can be ascribed to the shorter pore length in smaller carbon spheres. The capacitance values calculated from the inverse of slopes in Fig. 4 are also listed in Table 2. Obviously, the capacitance increases with an increase in the surface area of RF carbons. The *RC* time contants that were derived by a multiplication of ESR and capacitance are also listed in Table 2. The values steadily decrease with an increase in the pre-curing time, indicative of a better rate capability with a decrease in the carbon sphere size in this series of porous carbons.

In the previous reports, we demonstrated the usefulness of complex capacitance analysis for the assessment of EDLC parameters.[7,11,12] In this analysis, experimentally obtained impedance data are converted to complex capacitance and the imaginary part of complex capacitance is plotted as a function of frequency on a semi-logarithmic scale (imaginary capacitance plots, C_{im} vs. log f). The advantageous feature of this analysis over the conventional Nyquist plot (R_{im} vs. R_{re}) is that the capacitive component appears as a peak and the peak frequency (f_p) in imaginary capacitance plots has the following inverse relationship with time constant ($\tau = RC$)[7,12] :

$$\tau = \frac{0.404}{f_p}$$

Fig. 5 compares the imaginary capacitance plots derived from four RF carbon electrodes, where it seen that the capacitive peaks appear whose peak frequency gradually shifts toward the high frequency direction with an increase in the pre-curing time. The *RC* time constants derived from the above equation after locating the peak frequencies (f_p) in Fig. 5 were listed in Table 2. The values derived from two different experiments are fairly matched to each other within experi-

Table 2. Equivalent series resistance (ESR), capacitance and *RC* time constants that were obtained from the galvanostatic charge-discharge voltage profiles shown in Fig. 4

	RF00	RF30	RF60	RF90
ESR/Ωg	(8.8 ± 0.2) × 10^{-2}	(6.6 ± 0.2) × 10^{-2}	(3.9 ± 0.3) × 10^{-2}	(2.9 ± 0.1) × 10^{-2}
Capacitance/Fg^{-1}	93.3 ± 1.4	99.0 ± 2.7	111 ± 2.1	122 ± 0.9
Time constant [a]/s	8.2 ± 0.3 (8.4 ± 0.8)	6.5 ± 0.5 (5.5 ± 0.5)	4.3 ± 0.6 (3.6 ± 0.3)	3.6 ± 0.1 (2.4 ± 0.2)

[a] The values obtained from the imaginary capacitance plots (Fig. 5) are listed in the parentheses.

mental errors. Again, the smaller *RC* time constant (better rate capability) for the electrodes fabricated with smaller carbon spheres must be resulted from the smaller ESR, which is indebted to a facilitated ion penetration into shorter pores.

4. Conclusion

In this report, the preparation of spherical porous carbons and their rate capabiltiy as the EDLC electrodes were examined. The following points are sumarized:

(i) A series of spherical porous carbons that differ in the sphere size but are similar in the pore diameter were prepared. The carbon sphere size was controlled by changing the pre-curing time, which was possible by enforcing the acid-catalyzed condensation reaction by CTAB introduction after a pre-determined period of base-catalyzed addition reaction in the RF polymerization step. Similarity in the pore diameter of intra-particle pores was resulted from gasification inside the RF gels during the carbonization period. The sphere size, thus the pore length, steadily decreases with an increase in the pre-curing time.

(ii) The surfactant molecules play, in addition to the proton release by an electrostatic lipophilic interaction with RF clusters, important roles in this preparation. They form spherical micelles in water and act as a template for RF polymerization to produce the RF gels of a sphere shape, and minimize the pore collapse during drying step by lowering the surface tension at the pore water/gel interface.

(iii) The pore-length-dependent rate capability was demonstrated on the galvanostatic charge-discharge voltage profiles and imaginary capacitance plots. Two experimental results consistently illustrate that the rate capability becomes better with a decrease in the pore length, which is certainly indebted to facilitated ionic motions inside shorter pores.

Acknowledgement

This work was supported by KOSEF via the Research Center for Energy Conversion and Storage, and by the Division of Advanced Batteries in NGE Program (Project No. 10016439).

References

1. A. Nishino, "Capacitors: operating principles, current market and technical trends" *J. Power Sources*, **60**, 137 (1996).
2. S.-R. Hwang, H. Teng, "Capacitance enhancement of carbon fabric electrodes in electrochemical capacitors through electrodeposition with copper" *J. Electrochem. Soc.*, **149**, A591 (2002).
3. M. Winter, J. O. Besenhard, M. E. Spahr, P. Novak, "Insertion electrode materials for rechargeable lithium batteries" *Adv. Mater.*, **10**, 725(1998).
4. B. E. Conway, "*Electrochemical Supercapacitors*", Kluwer Academic/ Plenum Publisher, (1999).
5. R. Kötz, M. Carlen, "Principles and applications of electrochemical capacitors", *Electrochim. Acta*, **45**, 2483 (2000).
6. S. Yoon, J. Lee, T. Hyeon, S. M. Oh, "Electric double-layer capacitor performance of a new mesoporous carbon", *J. Electrochem. Soc.*, **147**, 2507 (2000).
7. S. Yoon, J. H. Jang, B. H. Ka, S. M. Oh, "Complex capacitance analysis on rate capability of electric-double layer capacitor (EDLC) electrodes of different thickness", *Electrochim. Acta*, **50**, 2255 (2005).
8. K. T. Lee, S. M. Oh, "Novel synthesis of porous carbons with tunable pore size by surfactant-templated sol-gel process and carbonization", *Chem. Commun.*, **21**, 2722 (2002).
9. N. Nishiyama, T. Zheng, Y. Yamane, Y. Egashira, K. Ueyama, "Microporous carbons prepared from cationic surfactant–resorcinol/ formaldehyde composites", *Carbon*, **43**, 269 (2005).
10. I. Matos, S. Fernandes, L. Guerreiro, S. Barata, A. M. Ramos, J. Vital, I. M. Fonseca, "The effect of surfactants on the porosity of carbon xerogels", *Micro & Mesoporous Materials*, **92**, 38 (2006).
11. J. H. Jang, S. M. Oh, "Complex capacitance analysis of porous carbon electrodes for electric double-layer capacitors", *J. Electrochem. Soc.*, **151**, A571 (2004).
12. J. H. Jang, S. Yoon, B. H. Ka,Y. H. Jung, S. M. Oh, "Complex capacitance analysis on leakage current appearing for electric double-layer capacitor electrode", *J. Electrochem. Soc.*, **152**, A1418 (2005).
13. R. W. Pekala, "Organic aerogels from polycondensation of resorcinol with formaldehyde", *J. Mater. Sci.*, **24**, 3221 (1989).
14. X. Lu, M. C. Arduini-Schuster, J. Kuhn, O. Nilsson, J. Fricke, R. W. Pekala, "Thermal conductivity of monolithic organic aerogels", *Science*, **255**, 971 (1992).
15. C. Lin, J. A. Ritter, "Effect of synthesis pH on the structure of carbon xerogels", *Carbon*, **35**, 1271 (1997).
16. H. Tamon, H. Ishizaka, "SAXS Study on Gelation Process in Preparation of Resorcinol–Formaldehyde Aerogel", *J. Colloid Interface Sci.*, **206**, 577 (1998).
17. S. A. Al-Muhtaseb, J. A. Ritter, "Preparation and properties of resorcinol- formaldehyde organic and carbon gels", *Adv. Mater.*, **15**, 101 (2003).
18. N. Job, R. Pirard, J. Marien, J. P. Pirard, "Porous carbon xerogels with texture tailored by pH control during sol-gel process", *Carbon*, **42**, 619 (2004).
19. Y. Tao, H. Kanoh, K. Kaneko, "Synthesis of Mesoporous zeolite A by resorcinol-formaldehyde templating", *Langmuir*, **21**, 504 (2005).
20. Y. Zhu, H. Hu, W. Li, X. Zhang, "Resorcinol-formaldehyde based porous carbon as an electrode material for supercapacitors", *Carbon*, **45**, 160 (2007).
21. G. Horvath, K. Kawazoe, "Method for the calculation effective pore size distribution in molecularsieve carbon", *J. Chem. Eng. Jpn.*, **16**, 470 (1983).
22. G. Horvath, "Energetic interactions in phase and molecular level pore characterisation in nano-range", *Colloids Surf. A*, **141**, 295 (1998).
23. J. H. de Boer, B. C. Lippens, B. G. Linsen, J. C. P. Broekhoff, A. van den Heuvel, Th. J. Osinga, "The *t*-curve of multimolecular N_2-adsorption", *J. Colloid Interface Sci.*, **21**, 405 (1966).
24. K. S. W. Sing, D. H. Evertt, R. A. W. Haul, L. Moscou, R. A. Pierotti, J. Rouquerol, T. Siemieniewska, "Reporting physisorption data for gas/solid systems with special reference to the determination of surface area and porosity", *Pure Appl. Chem.*, **57**, 603 (1985).
25. E. F. Sousa-Aguilar, A. Liebsch, B. C. Chaves, A. F. Costa, "Influence of the external surface area of small crystallite zeolites on the micropore volume determination", *Micropor. Mesopor. Mater.*, **25**, 185 (1998).
26. M. Itagaki, S. Suzuki, I. Shitanda, K. Watanabe, H. Nakazawa, "Impedance analysis on electric double layer capacitor with transmission line model", *J. Power Sources*, **164**, 415 (2007).
27. H. Y. Liu, K. P. Wang, H. Teng, "A simplified preparation of mesoporous carbon and the examination of the carbon accessibility for electric double layer formation", *Carbon*, **43**, 559 (2005).
28. X. P. Dong, W. H. Shen, J. L. Gu, L. M. Xiong, Y. F. Zhu, H. Li, J. L. Shi, "MnO_2-embedded-in-mesoporous-carbon-wall structure for use a electric double-layer capacitor", *J. Phys. Chem. B*, **110**, 6015 (2006).